

PCCP

Accepted Manuscript



This is an *Accepted Manuscript*, which has been through the Royal Society of Chemistry peer review process and has been accepted for publication.

Accepted Manuscripts are published online shortly after acceptance, before technical editing, formatting and proof reading. Using this free service, authors can make their results available to the community, in citable form, before we publish the edited article. We will replace this *Accepted Manuscript* with the edited and formatted *Advance Article* as soon as it is available.

You can find more information about *Accepted Manuscripts* in the [Information for Authors](#).

Please note that technical editing may introduce minor changes to the text and/or graphics, which may alter content. The journal's standard [Terms & Conditions](#) and the [Ethical guidelines](#) still apply. In no event shall the Royal Society of Chemistry be held responsible for any errors or omissions in this *Accepted Manuscript* or any consequences arising from the use of any information it contains.

Cite this: DOI: 10.1039/c0xx00000x

www.rsc.org/xxxxxx

ARTICLE TYPE

Use of silane-functionalized graphene oxide in organic photovoltaic cells and organic light-emitting diodes

Chang Yeong Lee, Quyet Van Le, Cheolmin Kim, and Soo Young Kim*

Received (in XXX, XXX) Xth XXXXXXXXXX 20XX, Accepted Xth XXXXXXXXXX 20XX

DOI: 10.1039/b000000x

Graphene oxide (GO) and silane-functionalized GO (sGO) sheets obtained through a simple sonication exfoliation method are employed as hole transport layers to improve the efficiency of organic photovoltaic cells (OPV) and organic light-emitting diodes (OLED). GO was functionalized using (3-glycidyloxypropyl)trimethoxysilane (GPTMS) and triethoxymethylsilane (MTES). The appearance of new peaks in the Fourier-transform infrared spectra of the sGOs indicates the formation of Si–O–C, Si–O–Si, Si–H, and Si–O–C moieties, which provide evidence of the addition of silane to the GO surface. Furthermore, the appearance of Si–O–Si bonds in the synchrotron radiation photoelectron spectroscopy (SRPES) data of the MTES-sGO and GPTMS-sGO samples suggests that silane groups were effectively functionalized onto the GO sheets. An OPV cell with GO layers showed a lower performance with a power conversion efficiency (PCE) of 2.06 %; in contrast, OPV cells based on GPTMS-sGO and MTES-sGO had PCE values of 3.00 and 3.08 %, respectively. The OLED devices based on GPTMS-sGO and MTES-sGO showed higher maximum luminance efficiency of 13.91 and 12.77 cd/A, respectively, than PEDOT:PSS-based device (12.34 cd/A). The SRPES results revealed that the work functions of GO, GPTMS-sGO, and MTES-sGO were 4.8, 4.9, and 5.0 eV, respectively. Therefore, the increase in the PCE value is attributed to improved band-gap alignment. It is thought that sGO could be used as interfacial layer in OPV and OLED devices.

1 Introduction

In recent years, organic photovoltaic (OPV) and organic light-emitting diode (OLED) devices have attracted much attention because of rapid energy payback time, light weight, flexibility, and ease of enlargement through a roll-to-roll coating process.¹⁻⁵ Further improvement of the efficiency, lower fabrication cost, and enhancement of the device stability at ambient conditions are important for commercial use of OPV and OLED devices.⁶⁻⁸ The use of a hole transport layer (HTL) in OPV and OLED devices could maximize the device efficiency. In OPV devices, the HTL should have a proper energy level alignment to improve hole extraction and selectively block electrons to reduce electron-hole recombination on the anode.⁹ Poly(3,4-ethylenedioxythiophene):poly(styrene sulfonate) (PEDOT:PSS) layers are widely used as HTLs. However, PEDOT:PSS has several undesirable properties including its acidic and hygroscopic nature, electrical and structural inhomogeneity, and poor electron-blocking properties.¹⁰⁻¹² Therefore, new material is needed to be used as HTL instead of PEDOT:PSS.

Graphene has attracted significant scientific interest because of its large surface area ($2630 \text{ m}^2 \text{ g}^{-1}$), high intrinsic mobility ($200000 \text{ cm}^2 \text{ v}^{-1} \text{ s}^{-1}$), high Young's modulus ($\sim 1.0 \text{ TPa}$), high thermal conductivity ($\sim 5000 \text{ W m}^{-1} \text{ K}^{-1}$), and high optical transmittance ($\sim 97.7 \%$).¹³⁻¹⁶ For low-cost mass production,

graphene oxide (GO) has attracted much attention. GO is an intriguing nanomaterial with tremendous potential for large-area electronics; it is also water dispersible and therefore solution processable. Thus, GO, reduced GO, and graphene have been reported as candidates for HTLs for high performance OPV and OLED devices instead of PEDOT:PSS.^{9, 17-20} GO contains many functional groups, such as hydroxyl, carboxyl, carbonyl, and epoxide, which enable surface functionalization for various applications.²¹⁻²³ Therefore, it is expected that the electronic properties of GO could be tuned via versatile functionalization of GO, which may lead to higher efficiency OPV, OLED devices and the widespread use of GO as HTLs in OPVs and OLEDs.

In this study, we investigated the effect of silane-functionalized GO (sGO) as HTLs in OPV and OLED devices to modify the metal anode contact. Functionalization of GO was achieved using (3-glycidyloxypropyl)trimethoxysilane (GPTMS) and triethoxymethylsilane (MTES). A simple spin-coating process was used to modify the ITO anode contact with sGO as the HTLs. The properties of sGO were examined using atomic force microscopy (AFM), X-ray diffraction (XRD), synchrotron radiation photoemission spectroscopy (SRPES), and ultraviolet photoemission spectroscopy (UPS). After application of sGO as the HTLs in OPV and OLED devices, the performances of the OPV and OLED devices were measured; thus, it was determined that sGO is more suitable for HTLs in OPV OLED devices than GO.

2 Experimental Section

2.1 Synthesis of GO

GO was prepared using a modified Hummers method.²⁴ Briefly, 2 g of graphite powder (Alfa Aesar, universal grade, 200 mesh, 99.9995 %) was stirred with 2 g of NaNO₃ and 100 mL of concentrated H₂SO₄ for one day in an ice water bath. After stirring, 12 g of KMnO₄ was gradually added. After mixing the solution well, the ice bath was removed and the solution was stirred at 35 °C until a highly viscous liquid was obtained. Following the sequential addition of 200 mL of pure water and H₂O₂, the mixture was centrifuged at 8000 rpm and washed with HCl and water. The centrifuging and washing process was repeated a few times. Finally, the GO was dried at 50 °C for 24 h in a vacuum oven.

2.2 Synthesis of sGO

GO sheets containing many oxygen groups (i.e., hydroxyl, carboxyl, and carbonyl groups on their basal planes and edges) were reacted with self-assembled monolayers (SAMs). To silanize GO, 20 mg GO was placed in a three-neck flask with 40 mL deionized (DI) water and dispersed through sonication for 60 min. Then, 5 mL of 0.2 M toluene solution containing the SAMs (GPTMS and MTES, Sigma-Aldrich) was added. The homogeneously dispersed GO, which was a brown solution, was stirred and heated at 70 °C for 24 h. After that, the color of mixture changed to dark brown, indicating the formation of sGO. The product was washed with ethanol and DI water and dried at 50 °C for 24 h in a vacuum oven. An ultrasonicator (Sonicator Microtip Probes, Sonics VCX-750, Sonics & Materials, Inc., USA) was used to exfoliate the GO and sGO powder. GO and sGO (10 mg) were each mixed with ethylene glycol (10 mL) in a 20 mL flask. The solution was sonicated at 300 W for 4 h, which were the optimal conditions for this experiment.

2.3 Fabrication of OPV and OLED devices.

A patterned indium tin oxide (ITO) glass substrate was utilized for OPV and OLED devices fabrication. First, the substrate was sequentially cleaned with acetone, isopropyl alcohol, and DI water for 15 min each with ultrasonic assistance. Then, the cleaned ITO glass was dried at 80 °C for 15 min before undergoing ultraviolet ozone (UVO) treatment for 15 min. Four types of OPV and OLED devices were fabricated. The ultra-thin layers of GO and sGO were spin-coated at 5000 rpm for 30 s in ethylene glycol. PEDOT:PSS was also spin-coated at 4000 rpm for 30 s. For OPV devices, Poly(3-hexylthiophene) (P3HT) and [6,6]-phenyl-C61-butyric acid methyl ester (PCBM), which were used as the donor and acceptor, respectively, in a 6:4 weight ratio with a concentration of 30 mg mL⁻¹ in 1,2-dichlorobenzene, were spin-coated at 700 rpm for 30 s and annealed at 110 °C for 10 min. For OLED devices, N,N-Di(1-naphthyl)-N,N'-diphenyl-(1,10-biphenyl)-4,40-diamine (NPB) (40 nm) as hole transport layer, tris-(8-hydroxyquinoline)aluminium (Alq₃) (host, 30 nm), 2,3,6,7-Tetrahydro-1,1,7,7-tetramethyl-1H, 5H, 11H-10-(2-benzothiazolyl)quinolizino[9,9a,1gh]coumarin (C545T) (dopant,

5% doping) as emitting layer, bathocuproine (BCP) (5 nm) as hole blocking layer, and Alq₃ (25 nm) as electron transport layer were deposited, respectively, under a vacuum of about 2×10^{-6} Torr each with deposition rate of 1 Å/s. Finally, the cathode comprising LiF (1 nm thickness) and Al (100 nm thickness) was thermally deposited with deposition rates of 0.1 Å/s and 10 Å/s, respectively. The active area of the OPV and OLED device were approximately 4 mm² and 9 mm², respectively. All devices were fabricated together for comparison.

2.4 Characterization

To confirm the characteristics of OPV devices, the current density–voltage (J–V) curves were measured under ambient air with glass encapsulation using a Keithley 2622A source measurement unit. Mask is used in measuring step for accurate data. To confirm the characteristics of OLED devices, a Keithley 2622A source meter and a MINOLTA CS100A luminance meter were used to measure the current-voltage-luminance characteristics and CIE chromaticity coordinates, respectively. Synchrotron radiation photoelectron spectroscopy (SRPES) experiments were performed in an ultrahigh vacuum chamber (base pressure of $\sim 10^{-10}$ Torr) in a 4D beamline equipped with an electron analyzer and a heating element at the Pohang Acceleration Laboratory. The onset of photoemission, which corresponds to the vacuum level at the surface of GO and sGO, was measured using an incident photon energy beam of 250 eV with a negative bias on the sample. The results were corrected for charging effects using Au 4f as an internal reference. For the Fourier-transform infrared (FT-IR) spectroscopy measurements, the synthesized materials were pressed into pellets with potassium bromide (KBr) and scanned using radiation ranging in frequency from 400 to 4000 cm⁻¹. Atomic force microscopy (AFM, XE-120, Park Systems Corp., Korea) in non-contact mode and field-emission scanning electron microscope (FE-SEM) were employed to confirm the morphology and thickness of the exfoliated GO and sGO layers.

3 Results and discussion

Figure 1 shows the FT-IR spectra of GO, MTES-sGO, and GPTMS-sGO. The chemical structures of MTES and GPTMS are shown in the inset of Figure 1. The peaks located at 3400, 1708, 1636, 1350, and 1230 cm⁻¹ in the GO spectrum indicate the presence of –OH, C=O, C=C, and C–O bonds, respectively, which suggests the existence of hydroxyl, carboxyl, and epoxide groups on the surface of GO. The spectra of the sGOs have several new peaks that are not present in the GO spectrum: The signals located at 2932 and 2880 cm⁻¹ correspond to the symmetric and asymmetric vibrations of alkyl groups, which are assigned to the silane moieties of the sGOs. The disappearance of the peaks located at 1708, 1350, and 1230 cm⁻¹ in the GO spectrum suggests that the carboxyl and epoxide groups of the GOs reacted with the silane groups of the SAMs. Moreover, the appearance of new peaks at 1124, 1030, 780, and 694 cm⁻¹ in the spectra of the sGOs indicates the formation of Si–O–C, Si–O–Si, Si–H, and Si–O–C, which is further evidence of the presence of silane on the GO surface.

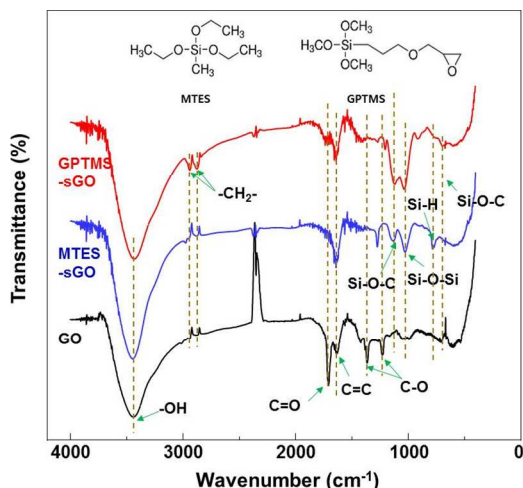


Fig. 1 FT-IR spectra of GO, GPTMS-sGO, and MTES-sGO.

Survey scans of the GO and GPTMS-sGO SRPES spectra are shown in Figure 2(a). The Si 2p peak is not present in the GO spectrum; however, it appears at 99.6 eV in the GPTMS-sGO spectrum, indicating that covalent functionalization of GO with the SAM was successful. Figure 2(b) shows C 1s and O 1s SRPES spectra of GO, MTES-sGO, and GPTMS-sGO. To separate the chemical bonding states, including those in the spectra, the spectral line shape was simulated using a suitable combination of Gaussian and Lorentzian functions.²⁰ The peak separation shown here is one of possible combinations. The C 1s spectra consist of various components, which are assigned to C-Si (283.6 eV), C-C/C=C (284.7 eV), C-O/C-O-Si (285.6 eV), C-O-C (286.4 eV), C=O (287.8 eV), and O-C=O (289.0 eV).²¹ The C-Si bonds that are present in the spectra of MTES-sGO and GPTMS-sGO at 283.6 eV are not present in the GO spectrum, confirming that MTES and GPTMS were grafted onto the surface of the GO. The O 1s spectra is separated into O-C=O (530.2 eV), C=O (531.2 eV), C-O/C-O-Si (532.3 eV), Si-O-Si (532.7 eV), and C-O-C (534 eV) components.²⁶⁻²⁷ The presence of Si-O-Si signals in the MTES-sGO and GPTMS-sGO spectra suggests that the silane groups were effectively functionalized onto the GO sheets.

Figure 3 shows the FE-SEM images of GO and MTES-sGO. The typical GO and sGO sizes were less than $2 \times 2 \mu\text{m}^2$. The MTES-sGO sample is smaller than the GO sample; this difference in flake size may arise from the pre-sonication process during the surface functionalization process (i.e., dispersion and silanization). According to AFM measurement (not shown here), the average thickness of the GO sheets is about 1 nm, which is in agreement with previous reports.²⁸ The average thickness of MTES-sGO is about 1.8 nm, indicating the addition of the SAM to the surface of GO. sGO is thicker than GO regardless of the SAM type, suggesting the presence of silane-functionalized groups on the GO sheets.

Figure 4 shows the work functions of GO, MTES-sGO, and GPTMS-sGO. The onsets of the secondary electrons were determined by extrapolating the two solid lines from the background and straight onset in the spectra.²⁹ GO has a work function of 4.8 eV. After chemical functionalization, the work

function increases to 4.9 and 5.0 eV for GPTMS-sGO and MTES-sGO, respectively. This result suggests that the use of sGO as a HTL could reduce the hole extraction barrier between the anode and active layers, thereby increasing the efficiency.

45

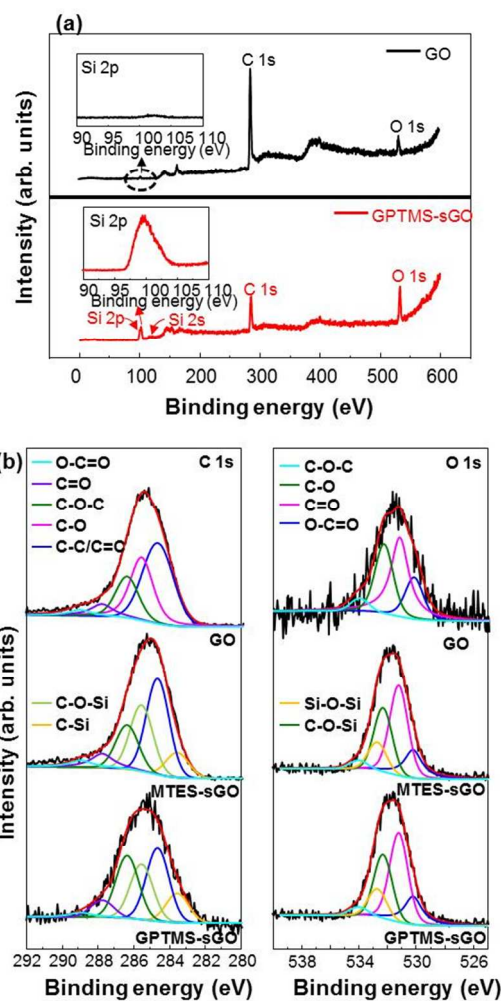


Fig. 2 (a) Survey curves of GO and GPTMS-sGO; inset: higher resolution of the Si 2p curves. (b) Higher resolution SRPES curves of C 1s and O 1s of GO, MTES-sGO, and GPTMS-sGO.

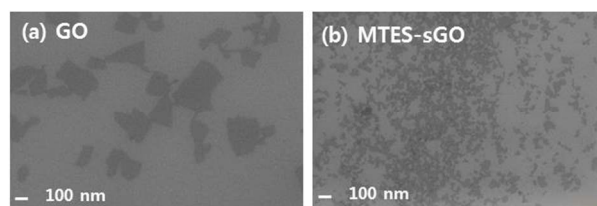


Fig. 3 FE-SEM images of (a) GO and (b) MTES-sGO sheets spin-coated onto SiO_2/Si substrates.

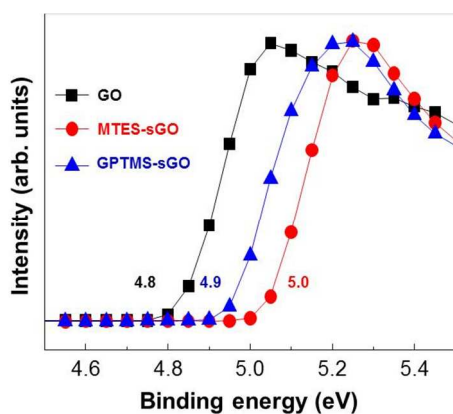


Fig.4 Changes in the onsets of the secondary electrons of GO, MTES-sGO, and GPTMS-sGO.

Figure 5(a) shows J–V curves of the OPV cells with different device structures. The experiments were performed at least five times to confirm the effect of sGO. Four devices are fabricated together each time and the data shown here are typical ones. The photocurrent was measured under AM 1.5G 100 mW cm⁻² illumination. The power conversion efficiency (PCE), open-circuit voltage (V_{oc}), short-circuit current density (J_{sc}), and fill factor (FF) were measured. The bare ITO-based OPV cell has a PCE of 1.56 % ($J_{sc} = 7.9$ mA cm⁻², $V_{oc} = 0.4$ V, and FF = 49 %). Insertion of a GO layer increases the PCE of the device slightly to 2.06 % ($J_{sc} = 7.07$ mA cm⁻², $V_{oc} = 0.62$ V, and FF = 47 %) because of the reduction of the energy barrier between the active layer and ITO. However, the performance of the GO-based device is still much lower than that of a PEDOT:PSS-based device (PCE = 3.29 %, $J_{sc} = 8.15$ mA cm⁻², $V_{oc} = 0.62$ V, and FF = 64 %) because of the low work function of GO. The PCE values of GPTMS-sGO- and MTES-sGO-based OPV cells increase to 3.0 and 3.08 %, respectively. A summary of the device properties is given in Table 1. It is thought that the increased work function of sGO reduces the hole extraction barrier, as shown in Figure 5(b), resulting in the improved PCE. The energy levels of ITO, PEDOT:PSS, P3HT:PCBM, and LiF/Al were obtained from other literature.³⁰⁻³¹ The performance of the sGO-based OPV cell is slightly lower than that of PEDOT:PSS-based OPV cells, suggesting that sGO can be used to replace PEDOT:PSS as the HTLs in high-performance OPV cells through a solution process.

Table 1 Summary of the OPV cells properties

	J_{sc} (mA m ⁻²)	V_{oc} (V)	FF (%)	PCE (%)
ITO	7.90	0.40	49	1.56
PEDOT:PSS	8.15	0.62	64	3.29
GO	7.07	0.62	47	2.06
MTES-sGO	7.63	0.62	65	3.08
GPTMS-sGO	7.78	0.60	64	3.00

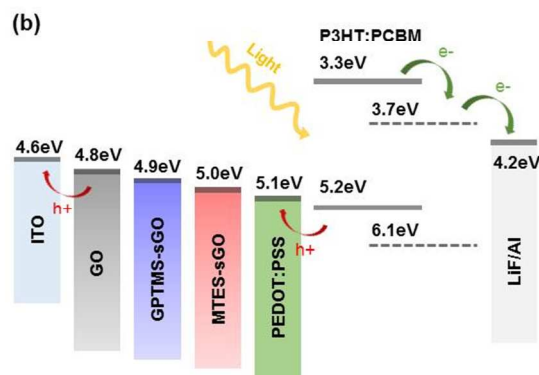
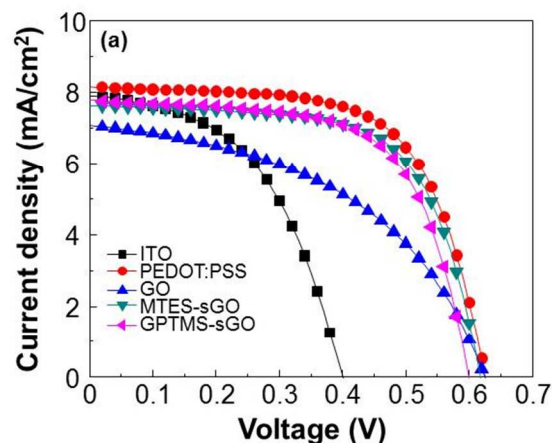


Fig.5 (a) J–V characteristics of devices without an interlayer and with GO, MTES-sGO, and GPTMS-sGO interlayers. (b) Schematic band diagram of the OPV cells.

Figure 6(a) and (b) shows the luminance-voltage characteristics and luminance efficiency of OLED devices. The device band diagram is shown in Figure 6(c). The turn on voltage at 10 cd/m² are 3.65, 4.15, 3.9, and 4.55 V for OLED devices using PEDOT:PSS, GO, MTES-sGO, and GPTMS-sGO as HTL materials, respectively. The higher turn on voltage of GPTMS-sGO-based OLED device than MTES-sGO-based device is due to its thicker thickness. The maximum luminance efficiency of the GO-based device (10.97 cd/A) is lower than that of a PEDOT:PSS-based device (12.34 cd/A) because of low work function of GO. In contrast, the efficiency of MTES-sGO- and GPTMS-sGO-based OLED devices are enhanced to 12.77 cd/A and 13.91 cd/A, respectively, as compared to PEDOT:PSS-based device in spite of higher turn on voltage. A summary of the device properties is given in Table 2. These results indicate that silane-functionalization of GO as HTL improves the charge balance in OLED device.

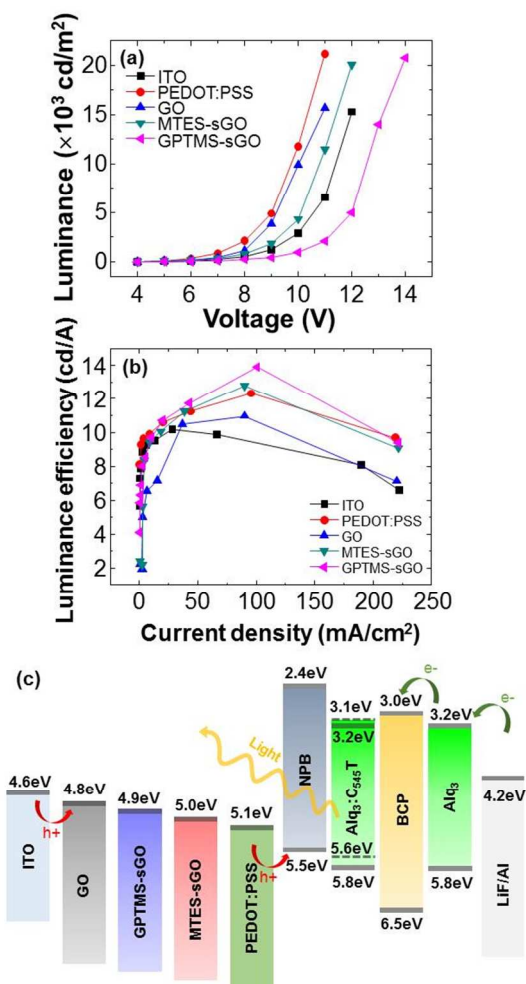


Fig.6 The (a) luminance–voltage and (b) luminance efficiency–current density characteristics of OLED devices with four different types of HTLs. (c) Schematic band diagram of the OLED devices.

Table 2 Summary of the OLED device properties

	Turn-on voltage (V)	Luminance max (cd/m ²)	Luminance Efficiency max (cd/A)	Power Efficiency max (lm/W)
ITO	4.35	15300	10.18	4.57
PEDOT:PSS	3.65	21200	12.34	6.37
GO	4.15	15700	10.97	3.65
MTES-sGO	3.9	20100	12.77	3.74
GPTMS-sGO	4.55	20800	13.91	3.68

4 Conclusions

In conclusion, we successfully developed a simple method to obtain chemically converted GO sheets via covalent functionalization with GPTMS and MTES. Silane was chemically grafted onto the GO sheets via the reaction of Si–OCH₃ groups with OH groups, and most of the residual oxygen-containing groups were removed to recover the sp²-network graphene. The FT-IR spectra indicated that the reaction between the alkyl and epoxy functional groups in the SAMs and hydroxyl groups of the GO surface occurred successfully. The appearance of C–Si, C–O–Si, and Si–O–Si peaks in the SPRES spectra confirmed the formation of sGO. Furthermore, the AFM images confirmed that MTES-sGO (1.8 nm) is thicker than GO (1 nm), indicating the addition of functional groups. The work function increased from 4.8 to 4.9 and 5.0 eV for GPTMS-sGO and MTES-sGO, respectively. Upon inserting the GO as the HTL in an OPV cell, the PCE slightly increased from 1.56 to 2.06 %, which was still much lower than that of PEDOT:PSS-based devices (PCE = 3.29 %) because of the low work function. The use of GPTMS-sGO and MTES-sGO sheets as the HTLs in OPV cells increased the PCE values to 3.00 and 3.09 %, respectively. It was proposed that the work function modulation of sGO enhanced its hole extraction properties. Also, we investigated device characteristics of OLEDs that are based on PEDOT:PSS, GO, GPTMS-sGO, and MTES-sGO as HTL. The efficiency of MTES-sGO- and GPTMS-sGO-based OLED devices are enhanced to 12.77 cd/A and 13.91 cd/A, respectively, as compared to PEDOT:PSS-based device due to suitable energy level alignment and improve charge balance. The improved performance of OPV and OLED which used thicker sGO comparing with thin GO suggested that the shifts in performance come from the existence of sGO. Therefore, it is expected that functionalization of GO could be highly desirable and beneficial for the future development of OPV and OLED devices with excellent efficiencies and stabilities.

Acknowledgement

This research was supported by the Mid-Career Research Program (2014R1A2A1A11051098) through the National Research Foundation of Korea (NRF), which is funded by the Ministry of Education, Science, and Technology.

Notes and references

⁴⁵ School of Chemical Engineering and Materials Science, Chung-Ang University 221, Heukseok-dong, Dongjak-gu, Seoul 156-756, Republic of Korea.

*E-mail: sooyoungkim@cau.ac.kr, Tel.: 82-2-820-5875, Fax: 82-2-824-3495.

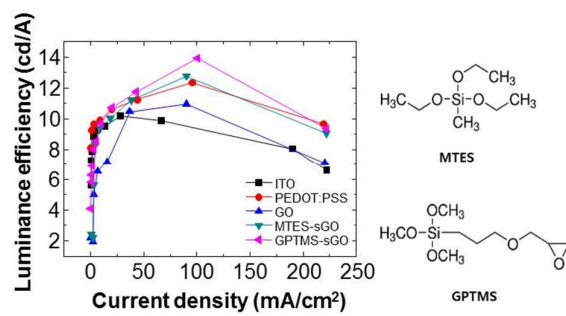
⁵⁰

- 1 S. B. Darling and F. You, *RSC Adv.*, 2013, **39**, 17633-17648.
- 2 H. Hoppe and N. S. Sariciftci, *J. Mater. Res.*, 2004, **19**, 1924-1945.
- 3 R. Søndergaard, M. Hösel, D. Angmo, T. T. Larsen-Olsen and F. C. Krebs, *Mater. Today*, 2012, **15**, 36-49.

⁵⁵

- 4 L. Xiao, Z. Chen, B. Qu, J. Luo, S. Kong, Q. Gong and J. Kido, *Adv. Mater.*, 2011, **23**, 926-52.
- 5 D. Yu, Y. Yang, M. Durstock, J. -B. Baek and L. Dai, *ACS Nano*, 2010, **4**, 5633-5640.
- 6 M. P. de Jong, L. J. van Ijzendoorn and M. J. A. de Voigt, *Appl. Phys. Lett.*, 2000, **77**, 2255.
- 7 M. Jørgensen, K. Norrman, S. A. Gevorgyan, T. Tromholt, B. Andreasen and F. C. Krebs, *Adv. Mater.*, 2012, **24**, 580-612.
- 8 F. C. Krebs, J. Fyenbo, D. M. Tanenbaum, S. A. Gevorgyan, R. Andriessen, B. van Remoortere, Y. Galagan, and M. Jørgensen, *Energy Environ. Sci.*, 2011, **4**, 4116.
- 9 J. Liu, G. H. Kim, Y. Xue, J. Y. Kim, J. B. Baek, M. Durstock and L. Dai, *Adv. Mater.*, 2014, **26**, 786-90.
- 10 S. K. Hau, H. -L. Yip, J. Zou and A. K. Y. Jen, *Org. Electron.*, 2009, **10**, 1401-1407.
- 11 M. Jørgensen, K. Norrman and F. C. Krebs, *Sol. Energy Mater. Sol. Cells*, 2008, **92**, 686-714.
- 12 L. S. C. Pingree, B. A. MacLeod and D. S. Ginger, *J. Phys. Chem. C*, 2008, **112**, 7922-7927.
- 13 A. A. Balandin, S. Ghosh, W. Bao, I. Calizo, D. Teweldebrhan, F. Miao and C. N. Lau, *Nano Lett.* 2008, **8**, 902-907.
- 14 K. I. Bolotin, K. J. Sikes, Z. Jiang, M. Klima, G. Fudenberg, J. Hone, P. Kim and H. L. Stormer, *Solid State Commun.*, 2008, **146**, 351-355.
- 15 C. Lee, X. Wei, J. W. Kysar and J. Hone, *Science* 2008, **321**, 385-8.
- 16 S. Morozov, K. Novoselov, M. Katsnelson, F. Schedin, D. Elias, J. Jaszczak and A. Geim, *Phys. Rev. Lett.*, 2008, **100**, 016602.
- 17 Y. Gao, H. -L. Yip, K. -S. Chen, K. M. O'Malley, O. Acton, Y. Sun, G. Ting, H. Chen and A. K. Y. Jen, *Adv. Mater.*, 2011, **23**, 1903-1908.
- 18 X. -C. Jiang, Y. -Q. Li, Y. -H. Deng, Q. -Q. Zhuo, S. -T. Lee and J. -X. Tang, *Appl. Phys. Lett.*, 2013, **103**, 073305.
- 19 S. -S. Li, K. -H. Tu, C. -C. Lin, C. -W. Chen and M. Chhowalla, *ACS Nano*, 2010, **4**, 3169-3174.
- 20 Y. Park, K. S. Choi and S. Y. Kim, *Phys. Status Solidi A*, 2012, **209**, 1363-1368.
- 21 D. R. Dreyer, S. Park, C. W. Bielawski and R. S. Ruoff, *Chem. Soc. Rev.* 2010, **39**, 228-40.
- 22 S. Park, and R. S. Ruoff, *Nat. Nanotechnol.*, 2009, **4**, 217-24.
- 23 S. Stankovich, D. A. Dikin, R. D. Piner, K. A. Kohlhaas, A. Kleinhammes, Y. Jia, Y. Wu, S. T. Nguyen and R. S. Ruoff, *Carbon*, 2007, **45**, 1558-1565.
- 24 W. S. Hummers and R. E. Offeman, *J. Am. Chem. Soc.*, 1958, **80**, 1339-1339.
- 25 X. Hu, E. Su, B. Zhu, J. Jia, P. Yao and Y. Bai, *Sci. Technol.*, 2014, **97**, 6-11.
- 26 L. Chen, H. Jin, Z. Xu, M. Shan, X. Tian, C. Yang, Z. Wang and B. Cheng, *Mater. Chem. Phys.*, 2014, **145**, 186-196.
- 27 D. Yang, A. Velamakanni, G. Bozoklu, S. Park, M. Stoller, R. D. Piner, S. Stankovich, I. Jung, D. A. Field, C. A. Ventrice Jr and R. S. Ruoff, *Carbon*, 2009, **47**, 145-152.
- 28 L. Zhang, J. Liang, Y. Huang, Y. Ma, Y. Wang and Y. Chen, *Carbon*, 2009, **47**, 3365-3368.
- 29 K. S. Choi, Y. Park and S. Y. Kim, *J. Nanosci. Nanotechnol.*, 2013, **13**, 3282-3287.
- 30 Q. V. Le, T. P. Nguyen, K. S. Choi, Y. -H. Cho, Y. J. Hong and S. Y. Kim, *Phys. Chem. Chem. Phys.*, 2014, **16**, 25468-25472.
- 31 Q. V. Le, T. P. Nguyen, H. W. Jang and S. Y. Kim, *Phys. Chem. Chem. Phys.*, 2014, **16**, 13123-8.

[Graphical Abstract]



The silane-functionalized graphene oxide could be used as interfacial layer in organic devices.